Colorless Coherent TDM-PON Based on a Frequency-Comb Laser

Md Mosaddek Hossain Adib ⓘ, *Student Member, IEEE*, Christoph Füllner ⓘ, *Student Member, IEEE*,
Juned N. Kemal ⓘ, Pablo Marin-Palomo ⓘ, Abderrahim Ramdane ⓘ, Christian Koos ⓘ,
Wolfgang Freude ⓘ, *Senior Member, IEEE*, and Sebastian Randel, *Senior Member, IEEE*

Abstract—Coherent reception becomes an interesting option when data rates in time-division-multiplexed (TDM) passive optical networks (PONs) grow beyond 50 Gbit/s. Controlling the wavelength, i.e., the optical frequency, and the phase of the laser acting as local oscillator (LO) is one of the main technical challenges in the design of coherent TDM PONs. In the optical network units (ONUs), low-cost lasers are required, which come at the expense of wavelength variations and drifts over multiple nanometers due to fabrication imperfections, and temperature variations. This contradicts the requirement of wavelength-stable LOs in coherent receivers. The use of a wavelength locker circuit and a temperature controller is considered as too complex for applications in access networks. In this work, we propose a novel colorless coherent architecture with high resilience to ONU laser wavelength drifts of up to ±4 nm (±0.5 THz) for future 100 Gbit/s PON. It allows the use of distributed feedback lasers at the ONU side. This is rendered possible by generating a frequency comb with carefully chosen free spectral range in a quantum-dash mode-locked laser diode at the optical line terminal. In upstream operation, the frequency comb serves as an LO, whereas the same information is modulated onto all comb lines for the case of downstream. As a result, the ONU laser can drift over the entire comb bandwidth without substantial performance penalty. We experimentally demonstrate downstream and upstream operation with an aggregated raw data rate of 96 Gbit/s, respectively. We further introduce advanced digital signal processing (DSP) methods including a coarse frequency offset compensation (CFOC) and a multiple-input multiple-output (MIMO) equalizer to improve the performance of our concept. We show that the receiver sensitivity can be increased by 3 dB for a high-bandwidth receiver when using a 6 × 2 MIMO equalizer scheme. A 4 × 2 MIMO equalizer scheme enables colorless reception even with a limited-bandwidth receiver.

Index Terms—DFB laser, coherent PON, frequency comb, PON, local oscillator.

I. INTRODUCTION

FUTURE optical access networks need to support the simultaneous operation of distinct service classes featuring a wide range of applications ranging from teleoperation of automated vehicles to cloud storage and the Internet of Things [1]. Thereby, each service class comes with its own traffic pattern and requirements in terms of bandwidth, latency and cost. Passive optical networks (PONs) based on statistical time-division multiplexing (TDM) are expected to play a key role in this scenario since they allow statistical multiplexing gains through dynamic bandwidth allocation [2]. This results in an efficient use of the fiber infrastructure resulting in significant cost advantages compared to point-to-point fiber links and static wavelength-division multiplexing. While PONs operating at a shared gross bit rate of 50 Gbit/s are currently being standardized, data rates of 100 Gbit/s and beyond will be required in the future [3]–[5]. In order to facilitate a smooth market introduction, coexistence with legacy PONs having a loss budget in the order of 30 dB, allowing a split factor of 64 or more, is required [6]–[8].

Conventional PONs rely on intensity modulation and direct detection (IM/DD) [3], [8]. However, with increasing symbol rates, the drawbacks of IM/DD, namely the limited receiver sensitivity and the lack of digital chromatic-dispersion (CD) compensation capabilities become relevant. On top of that, 100 Gbit/s IM/DD systems place high demands on the analog bandwidth of the transceiver components such as photodiodes (PDs), trans-impedance amplifiers (TIAs), digital-to-analog converters (DACs), and analog-to-digital converters (ADCs) [4], [5]. Coherent receivers in combination with inphase/quadrature (I/Q) modulation and polarization-division multiplexing (PDM) are considered a promising alternative [9]. They not only allow for reduced component bandwidth by distributing the data onto all four dimensions of the optical field but they also offer improved receiver sensitivities and they allow for digital CD compensation [9]–[12]. However, these benefits come at the price of an increased transceiver complexity [10]–[13]. Several promising

Md Mosaddek Hossain Adib, Christoph Füllner, Christian Koos, Wolfgang Freude, and Sebastian Randel are with the Institute of Photonics and Quantum Electronics, Karlsruhe Institute of Technology, 76131 Karlsruhe, Germany (e-mail: md.adib@kit.edu; christoph.fuellner@kit.edu; christian.koos@kit.edu; wolfgang.freude@kit.edu; sebastian.randel@kit.edu).

Juned N. Kemal was with the Institute of Photonics and Quantum Electronics, Karlsruhe Institute of Technology, 76131 Karlsruhe, Germany. He is now with the Vanguard Automation, Karlsruhe, Germany (e-mail: juned.kemal@vanguard-automation.com).

Pablo Marin-Palomo was with the Institute of Photonics and Quantum Electronics, Karlsruhe Institute of Technology, 76131 Karlsruhe, Germany. He is now with the Brussels Photonics (B-Phot), Vrije Universiteit Brussel, Belgium (e-mail: pablo.marin-palomo@vub.be).

Abderrahim Ramdane is with the Centre de Nanosciences et de Nanotechnologies CNRS, Université Paris-Saclay, 91220 Palaiseau cedex, France (e-mail: abderrahim.ramdane@c2n.upsaclay.fr).

Color versions of one or more figures in this article are available at https://doi.org/10.1109/JLT.2022.3164168.

Digital Object Identifier 10.1109/JLT.2022.3164168

concepts which simplify the coherent receiver architecture at the optical network unit (ONU) have been proposed in literature [9]–[17]. Furthermore, the progress in electronic-photonic integration technology promises a considerable complexity reduction of coherent receivers in the near future [18]–[20]. For instance, in [21], [22], a monolithically integrated coherent receiver including TIAs on silicon and an InP-based photonic integrated circuit consisting of a distributed-feedback (DFB) laser integrated with an I/Q modulator have been demonstrated. Yet, an unsolved challenge in coherent PONs is the precise wavelength matching required between the local oscillator (LO) and the transmit laser [5], [20], [23]. For that reason, tunable external-cavity lasers (ECLs) including a wavelength locker are usually employed in metro networks, long-haul networks, and in data center interconnects. However, ECLs are not an attractive option for PONs, especially for ONUs, where DFB lasers are preferred [5], [19], [20], [23]. However, due to fabrication constraints and imperfections, the wavelength of low-cost DFB lasers typically varies from batch to batch within ± 4nm [24]–[26]. Moreover, if operated uncooled, their wavelength is subject to temperature-induced wavelength drifts in the order of 0.1 nm/^{o}C [24]–[27]. Several approaches such as injection-locking [28] and reflective semiconductor optical amplifiers [29] have been proposed as potential solutions to this problem. In [30], [31], a fast tuning local oscillator has been demonstrated for burst-mode coherent receivers, however, low-cost fabrication of such fast-tuning lasers remains a technical hurdle [30].

In this work, we address the challenge of wavelength matching between the lasers in the optical line terminal (OLT) and in the ONUs. We propose a novel colorless coherent TDM-PON architecture that relies on a frequency comb source in the OLT and on low-cost uncooled DFB lasers in the ONUs. All lasers can be shared between up- and downstream operation, offering a trade-off between the overall system complexity and available optical power. This work is an extension of the authors work in [32], where 48Gbit/s upstream operation was experimentally demonstrated using an Erbium glass oscillator (ERGO) as a frequency comb source with a free-spectral range (FSR) 12.5GHz as LO. In this work, a quantum-dash (QD) mode-locked laser diode (MLLD) is used to generate the frequency comb. Its FSR of about 25GHz allows for higher data rates and its compactness is promising with respect to photonic-electronic integration. Initial results on that scheme have been reported in [33]. We experimentally demonstrate both up- and downstream operation, with an aggregated raw data rate of 96Gbit/s. Furthermore, we introduce advanced digital signal processing (DSP) schemes including a coarse frequency offset compensation (CFOC), spectral shifting of signal copies combined with multiple-input multiple-output (MIMO) equalization: while a 6×2 MIMO equalizer improves the receiver sensitivity by up to 3dB compared to a conventional 2×2 MIMO system, it requires an increased receiver bandwidth. Here, we therefore propose using a 4×2 MIMO equalizer instead which does not require an increased receiver bandwidth. For application in intra-datacenter interconnections, a related DSP scheme based on pilot-tone-assisted frequency offset compensation was recently published in [34]. With the proposed
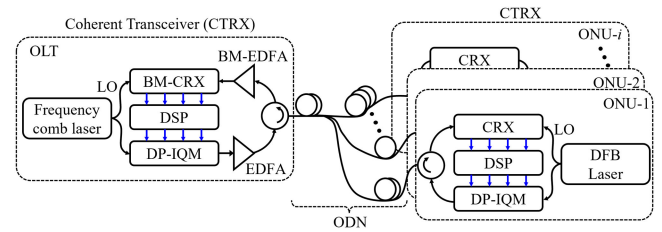

Fig. 1. Schematic of the proposed colorless coherent TDM-PON architecture. A C-band frequency comb source is shared between transmitter and receiver at the OLT. In downstream direction, a continuous-mode EDFA is used as booster amplifier, while in upstream direction, a burst-mode (BM) EDFA is used as a pre-amplifier. In the ONU transceiver, we consider shared C-band DFB lasers for up- and downstream operation. The coherent transceivers include dual-polarization I/Q modulators (DP-IQM), polarization diverse coherent receivers (CRX), as well as digital signal processing (DSP) logic.

architecture, we achieve a similar receiver sensitivity as with conventional DSP, but without the need for wavelength-locked lasers.

II. COLORLESS COHERENT TDM-PON ARCHITECTURE

The proposed colorless coherent TDM-PON architecture is illustrated in Fig. 1, with the OLT on the left-hand side and the ONUs on the right-hand side. In the OLT, the output of a frequency comb source is split in order to simultaneously act as a light source for the downstream signal and as a LO for the upstream signal. A dual-polarization I/Q modulator (DP-IQM) biased at the null point allows access to all four physical dimensions in a single-mode fiber. An Erbium-doped fiber amplifier (EDFA) operated in continuous mode is used to boost the downstream signal before it is sent to the optical distribution network (ODN) through a circulator. In upstream direction, a burst-mode EDFA acts as a pre-amplifier before the signal is detected by a burst-mode coherent receiver (BM-CRX) [35], [36].Details about the burst-mode EDFA can be found in [37]. Digital signal processing is carried out in an integrated complementary metal-oxide-semiconductor (CMOS) circuit for the OLT, which also includes an appropriate client interface. In the ONUs, a single DFB laser simultaneously acts as a light source for the upstream signal and as LO for the downstream. A DP-IQM is used to modulate all four dimensions in upstream operation and a coherent receiver (CRX) is used to receive the continuous downstream signal. Again, up- and downstream signals are interfaced to the ODN with a circulator. Another integrated CMOS circuit performs the required DSP at the ONUs. In bi-directional fiber links, multipath interference and Rayleigh back scattering can result in performance degradations. For a more detailed discussion and potential solutions, we refer to [38], [39].

III. THEORETICAL SYSTEM MODEL

In this section we briefly review single-line and multi-line laser sources before we discuss in detail the downstream and upstream operation of our proposed TDM-PON architecture.

A. Laser Sources

As discussed in Section II, we use a frequency comb source at the OLT, whereas we use single-line DFB lasers at the ONUs. For clarity, we introduce simplified models for single-line and frequency-comb sources in the following.

1) Single-Line Laser: We first consider a single-line laser emitting optical power P_L at optical frequency f_L. For convenience, we neglect amplitude noise, since it does not represent a dominant impairment in our application, and we describe the phase evolution due to phase noise and frequency drift by $\phi_L(t)$. The optical field can be expressed as

$$\underline{E}_L(t) = \sqrt{P_L}\, e^{j[2\pi f_L t + \phi_L(t)]}. \tag{1}$$

2) Multi-Line Source: The simplest way to generate a multi-line source is by combining multiple single-line lasers. For a source with $2N + 1$ laser lines, the optical field can thus be described as

$$\underline{E}_L(t) = \sum_{n=-N}^{N} \sqrt{P_L^{(n)}}\, e^{j[2\pi f_L^{(n)} t + \phi_L^{(n)}(t)]}. \tag{2}$$

where $P_L^{(n)}$, $f_L^{(n)}$, and $\phi_L^{(n)}$ describe the optical power, the frequency, and the phase evolution of the n-th laser line.

3) Frequency Comb Source: We refer to a multi-line source as a frequency comb source where the spectral lines have a nominally constant frequency spacing Δf_{FSR}, known as the free-spectral range (FSR), such that $f_L^{(n)} = f_L + n\Delta f_{FSR}$ and

$$\underline{E}_L(t) = \sum_{n=-N}^{N} \sqrt{P_L^{(n)}}\, e^{j[2\pi n\Delta f_{FSR} t + \phi_L^{(n)}(t)]}\, e^{j2\pi f_L t}. \tag{3}$$

4) Coherent Frequency Comb Source: If we assume that as the spectral lines of the frequency comb follow the same phase evolution $\phi_L(t)$ eventually with a constant phase offset $\Delta\phi_L^{(n)}$ for the n-th line, we call the multi-line laser a coherent frequency comb source. In this case, the optical field can be written as

$$\underline{E}_L(t) = \sum_{n=-N}^{N} \sqrt{P_L^{(n)}}\, e^{j[2\pi n\Delta f_{FSR} t + \Delta\phi_L^{(n)}]}\, e^{j[2\pi f_L t + \phi_L(t)]}. \tag{4}$$

If the phase offsets $\Delta\phi_L^{(n)}$ are all equal for all lines, the coherent frequency comb source is referred to as transform-limited. An example is a mode-locked laser, which generates a transform-limited frequency comb. Subsequent optical components might then lead to non-equal phase offsets $\Delta\phi_L^{(n)}$, e.g., due to CD.

B. Colorless Coherent Downstream

In a more detailed model for downstream (DS) operation, the relevant quantities are marked by $[\cdot]^{\downarrow}$. As shown in Fig. 2, the output of the frequency comb source in the OLT as explained with (4) is launched into a DP-IQM. Insets Ⓐ and Ⓑ show schematics of the power spectra at the input and at the output of the DP-IQM, respectively. We assume real electrical filter with a bandwidth Δf_{TX} for both the I and Q components, so that the optical signal bandwidth $\Delta f_{Sig} = 2\Delta f_{TX}$.
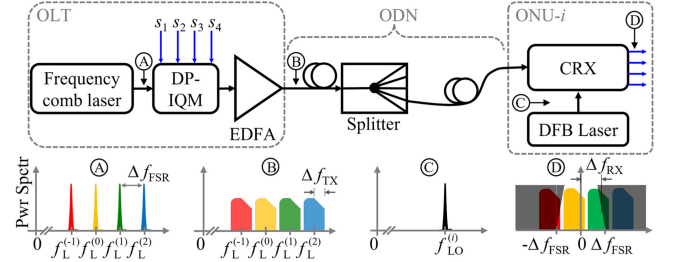

Fig. 2. Downstream schematic of the proposed coherent PON. At the OLT, we use a coherent frequency comb laser with an FSR of Δf_{FSR}. Using a dual-polarization I/Q modulator (DP-IQM), the downstream signal is modulated onto each comb line. Subsequently, an EDFA is used to boost the resulting optical signal to the required transmit power. Insets Ⓐ and Ⓑ illustrate the optical power spectra of the coherent comb laser and of the modulated transmit signal, respectively. In Ⓑ, $2\Delta f_{TX}$ indicates the optical bandwidth of the comb lines modulated with complex modulation signals $\underline{s}_{x,y}(t)$, which has to be smaller than Δf_{FSR}. At each ONU, we use a polarization-diverse coherent receiver (CRX) and a distributed feedback (DFB) laser as an LO. Inset Ⓒ illustrates the optical spectrum of the LO with an exemplary frequency offset. Inset Ⓓ shows the resulting baseband spectrum of the complex-valued received signals. The shaded regions illustrate the effect of the receiver's electrical bandwidth Δf_{RX}.

The DS signal $\underline{s}_{x,y}^{\downarrow}(t)$ is modulated on the frequency comb $\underline{E}_{L,x,y}^{\downarrow}(t)$ using DP-IQM. The output signal $\underline{E}_{Sig,x,y}^{\downarrow}(t)$ follows the liner modulation characteristics. In order to avoid spectral overlap, the bandwidth Δf_{Sig} of the transmit signal needs to be smaller than the FSR of the source, i.e., $2\Delta f_{TX} \leq \Delta f_{FSR}$. Notice that each comb line is modulated by the same data signal, and hence, each spectral line carries the same information. By tailoring the spectrum of the comb laser, compatibility with existing PON standards can be ensured. Next, we boost the power of resulting optical signal $\underline{E}_{Sig,x,y}^{\downarrow}(t)$ with an EDFA. Within its gain window (typically in the range of 30 nm [40]), the EDFA with power gain $G_A^{\downarrow} > 1$ adds amplified spontaneous emission (ASE) noise $\underline{E}_{ASE,x,y}^{\downarrow}(t)$ to the signal. Optionally, an optical filter, which passes the modulated comb lines only, could be added to limit the noise bandwidth. The combined effect of EDFA bandwidth and optional filter is described by the optical impulse response $\underline{h}_o^{\downarrow}(t)$. The symbol $*$ describes convolution. The amplified DS signal $\underline{E}_{x,y}^{\downarrow}(t)$ at point Ⓑ in Fig. 2 can thus be expressed as

$$\underline{E}_{x,y}^{\downarrow}(t) = \left[\sqrt{G_A^{\downarrow}}\, \underline{E}_{Sig,x,y}^{\downarrow}(t) + \underline{E}_{ASE,x,y}^{\downarrow}(t)\right] * \underline{h}_o^{\downarrow}(t). \tag{5}$$

The complex noise term $\underline{E}_{ASE,x,y}^{\downarrow}(t)$ is modelled by zero-mean circularly-symmetric additive white Gaussian noise (AWGN). At the ith ONU, we consider a DFB laser as the local oscillator and a balanced polarization-diverse coherent receiver. Inside the ODN, the power "gain" $G_{ODN}^{(i)} < 1$ describes the ODN power loss from point Ⓑ at the OLT to the ith ONU input of the balanced photodiode. The corresponding fiber impulse responses connect the un-primed polarizations and the primed received polarizations, $\underline{h}_{x'x}^{(i)}(t), \underline{h}_{x'y}^{(i)}(t), \underline{h}_{y'x}^{(i)}(t), \underline{h}_{y'y}^{(i)}(t)$, including the effect of chromatic dispersion (CD) and polarization rotation (PR). The optical signals $\underline{E}_{x',y'}^{\downarrow(i)}$ received in x′, y′ polarizations by the photodetectors of the balanced receivers in the ith ONU

are described by the following equations

$$\underline{E}_{x'}^{\downarrow(i)}(t) = \sqrt{G_{\mathrm{ODN}}^{(i)}} \left[\underline{h}_{x'x}^{(i)}(t) * \underline{E}_{x}^{\downarrow}(t) + \underline{h}_{x'y}^{(i)}(t) * \underline{E}_{y}^{\downarrow}(t) \right], \quad (6)$$

$$\underline{E}_{y'}^{\downarrow(i)}(t) = \sqrt{G_{\mathrm{ODN}}^{(i)}} \left[\underline{h}_{y'x}^{(i)}(t) * \underline{E}_{x}^{\downarrow}(t) + \underline{h}_{y'y}^{(i)}(t) * \underline{E}_{y}^{\downarrow}(t) \right]. \quad (7)$$

A schematic of the power spectrum of the LO is shown in Fig. 2 inset Ⓒ, centered at an exemplary frequency $f_{\mathrm{LO}}^{(i)}$, which can take arbitrary values within the range of the modulated comb spectrum at point Ⓑ. The mathematical descriptions of a single-line LO for the ith ONU in x′- and y′-polarization is in analogy to (1)

$$\underline{E}_{\mathrm{LO},x',y'}^{(i)}(t) = \sqrt{P_{\mathrm{LO}}^{(i)}}\, \mathrm{e}^{\mathrm{j}\left[2\pi f_{\mathrm{LO}}^{(i)} t + \phi_{\mathrm{LO}}^{(i)}(t)\right]}. \quad (8)$$

In the ONU receiver, the LO mixes with the received downstream signal in balanced photodetectors, resulting in the electrical data signals $\underline{r}_{x',y'}^{(i)}(t)$. The combined effect of shot noise and thermal noise $\underline{n}_{x',y'}^{(i)}(t)$ is added. The quantity $h_{\mathrm{RX}}^{(i)}(t)$ for the ith ONU represents the real electrical impulse responses for the I and Q signals in x′- and y′-polarization. The corresponding transfer functions are assumed to be identical with a single-sided bandwidth Δf_{RX}. Furthermore, $R^{(i)}$ is a constant conversion factor including the responsivity and the gain of the electrical amplifiers for all balanced receivers. The resulting received electrical signal is

$$\underline{r}_{x',y'}^{(i)}(t) = \left[R^{(i)} \underline{E}_{\mathrm{LO},x',y'}^{(i)}(t) \underline{E}_{x',y'}^{\downarrow(i)}(t) + \underline{n}_{x',y'}^{(i)}(t) \right] * h_{\mathrm{RX}}^{(i)}(t) \quad (9)$$

Fig. 2 inset Ⓓ illustrates the power spectrum of the received complex electrical signal at the ith ONU. The shaded region illustrates the effect of the receiver's low-pass characteristics. To avoid cost issues, no EDFA is put in front of the ONU. Therefore we expect that LO shot noise and thermal noise from the electronic circuits are the dominating noise sources. Using DSP, the impairments caused by CD and PR as well as bandwidth limitations of the transmitter and the receiver can be compensated to a large extent. If the transmit signal is boosted above a certain power level, we also expect impairments from fiber nonlinearities which are more difficult to mitigate.

C. Colorless Coherent Upstream

Fig. 3 shows a simplified model for the upstream (US) operation. The US relevant quantities are marked by $[\cdot]^{\uparrow}$. At the ONU, a DFB laser acts as the transmit laser defined in analogy to (8). Inset Ⓐ of Fig. 3 shows a schematic of the power spectrum of a single-line laser as seen at position Ⓐ in Fig. 3. The US signal $\underline{s}_{x',y'}^{\uparrow}(t)$ is modulated onto this carrier $\underline{E}_{\mathrm{L},x',y'}^{(i)}(t)$ using a DP-IQM. The modulated US optical signal $\underline{E}_{x',y'}^{\uparrow(i)}(t)$ from the ith ONU is launched into the ODN and transmitted in bursts as a TDM signal. The DP-IQM follows the linear modulation characteristics. The power spectrum of the modulated signal at position Ⓑ in Fig. 3 is shown in inset Ⓑ. The quantity $\Delta f_{\mathrm{TX}} \leq \frac{1}{2}\Delta f_{\mathrm{FSR}}$ corresponds to the bandwidth of the complex transmitted signal. The optical signal from the ith ONU received at the OLT can be written with definitions in analogy to (6)–(7). However, while
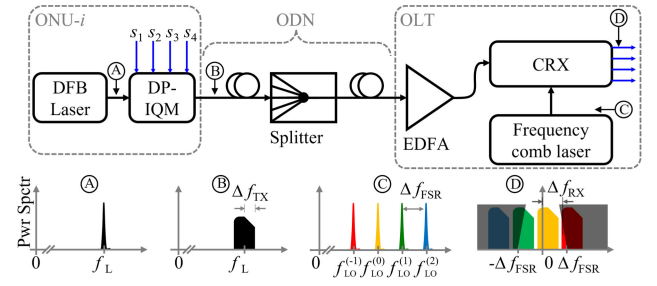

Fig. 3. Upstream schematic of the proposed coherent PON. At the ONU transmitter, we use a DFB laser which is followed by a DP-IQM. Insets Ⓐ and Ⓑ illustrate the optical spectra of the DFB laser and of the modulated signal, respectively. At the OLT side, we use a EDFA as a pre-amplifier, a coherent receiver (CRX) and a coherent frequency comb laser as an LO with an FSR of Δf_{FSR}. Inset Ⓒ, illustrates the optical spectrum of the LO frequency comb and inset Ⓓ shows the baseband spectrum of the complex-valued received signals. The shaded regions illustrate the effect of the receiver's electrical bandwidth Δf_{RX}.

the ONU sends out signals in x′- and y′-polarizations, the OLT receives them in x″- and y″-polarizations

$$\underline{E}_{\mathrm{Sig},x''}^{\uparrow(i)}(t) = \sqrt{G_{\mathrm{ODN}}^{(i)}} \left[\underline{h}_{x''x}^{(i)}(t) * \underline{E}_{x'}^{\uparrow(i)}(t) + \underline{h}_{x''y}^{(i)}(t) * \underline{E}_{y'}^{\uparrow(i)}(t) \right], \quad (10)$$

$$\underline{E}_{\mathrm{Sig},y''}^{\uparrow(i)}(t) = \sqrt{G_{\mathrm{ODN}}^{(i)}} \left[\underline{h}_{y''x}^{(i)}(t) * \underline{E}_{x'}^{\uparrow(i)}(t) + \underline{h}_{y''y}^{(i)}(t) * \underline{E}_{y'}^{\uparrow(i)}(t) \right]. \quad (11)$$

The EDFA pre-amplifier with power gain $G_{\mathrm{A}}^{\uparrow(i)} > 1$ adds ASE noise $\underline{E}_{\mathrm{ASE},x'',y''}^{\uparrow(i)}(t)$ as discussed in Section III-B. The ASE noise power spectral density depends on the instantaneous optical power of the upstream signal and EDFA gain $G_{\mathrm{A}}^{\uparrow(i)}$. The pre-amplified US signal at the OLT reads

$$\underline{E}_{x'',y''}^{\uparrow(i)}(t) = \left[\sqrt{G_{\mathrm{A}}^{\uparrow(i)}} \sum_i \underline{E}_{\mathrm{Sig},x'',y''}^{\uparrow(i)}(t) + \underline{E}_{\mathrm{ASE},x'',y''}^{\uparrow(i)}(t) \right] * \underline{h}_{o}^{\uparrow}(t). \quad (12)$$

At the OLT side, we consider a frequency comb laser source as an LO and a balanced polarization-diverse coherent receiver (CRX). The mathematical descriptions of a LO comb for the OLT in x″- and y″-polarization is in analogy to (4),

$$\underline{E}_{\mathrm{LO},x'',y''}(t) = \sum_{n=-N}^{N} \sqrt{P_{\mathrm{LO}}^{(n)}}\, \mathrm{e}^{\mathrm{j}\left[2\pi n\Delta f_{\mathrm{FSR}} t + \Delta\phi_{\mathrm{LO}}^{(n)}\right]} \mathrm{e}^{\mathrm{j}\left[2\pi f_{\mathrm{LO}} t + \phi_{\mathrm{LO}}(t)\right]}. \quad (13)$$

Fig. 3 inset Ⓒ illustrates the power spectrum of the LO at position Ⓒ. In the balanced photodetectors of the OLT CRX, the LO comb mixes with the pre-amplified US signal. The quantity R is a constant conversion factor including the responsivity and the gain of the electrical amplifiers of the CRX. The received electrical signal can be written as

$$\underline{r}_{x'',y''}(t) = \left[R\underline{E}_{\mathrm{LO},x'',y''}(t) \underline{E}_{x'',y''}^{\uparrow(i)}(t) + \underline{n}_{x'',y''}(t) \right] * h_{\mathrm{RX}}(t). \quad (14)$$

Fig. 3 inset Ⓓ illustrates the power spectrum of the complex received electrical signal measured at position Ⓓ. The shaded regions represent the effect of the low-pass characteristic of the
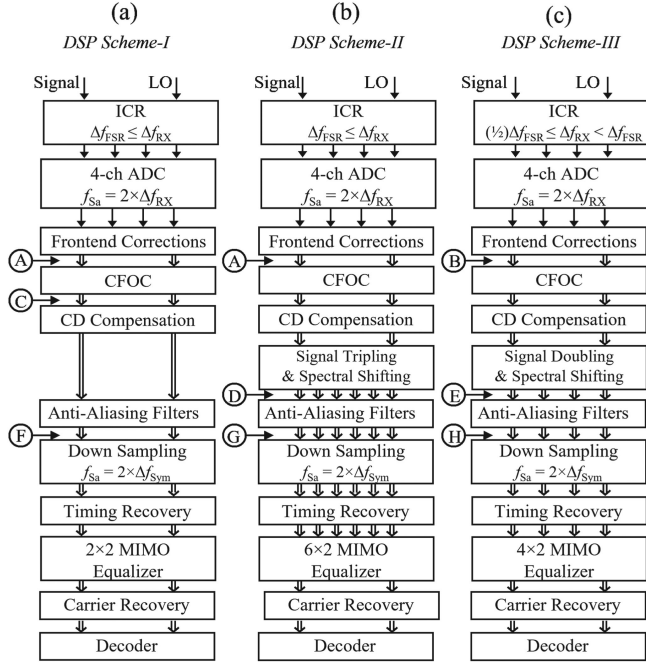
Fig. 4. Three different DSP schemes: (a) Reference scheme with 4-channel ADC and a sampling rate two times the electrical bandwidth Δf_{RX} of the receiver, followed by a coarse frequency offset compensation (CFOC), chromatic dispersion (CD) compensation, and anti-aliasing filters. The reduced-bandwidth signal is down-sampled with a sampling rate f_{Sa} two times the symbol rate Δf_{Sym}, which is in practice slightly smaller than the Nyquist rate Δf_{RX}. Timing recovery, multiple-input multiple-output (MIMO) equalization, carrier recovery, and finally demapping and decoding concludes the DSP chain. This scheme requires a receiver bandwidth of $\Delta f_{RX} \geq \Delta f_{FSR}$. (b) Advanced DSP scheme with signal tripling, spectral sifting by $\pm \Delta f_{FSR}$ and 6×2 MIMO equalizer, which again requires a receiver bandwidth of $\Delta f_{RX} \geq \Delta f_{FSR}$. (c) The DSP scheme with signal doubling, spectral shifting by $+\Delta f_{FSR}$ or $-\Delta f_{FSR}$ and 4×2 MIMO equalization. Here, the receiver bandwidth requirement is reduced to $\Delta f_{FSR} > \Delta f_{RX} \geq \frac{1}{2}\Delta f_{FSR}$. Notice that single-line arrows represent real-valued signals whereas double-line arrows represent complex-valued signals.

OLT receiver. The pre-amplifier at the OLT side adds ASE noise so that the ASE-LO beat noise is expected to dominate over the combined thermal noise and shot noise in $\underline{n}_{x'',y''}(t)$.

IV. DSP FOR COLORLESS COHERENT RECEPTION

This section provides a detailed discussion of the DSP schemes at the receivers in the ONUs and in the OLT, respectively. According to above assumptions and in contrast to ordinary heterodyne reception, the LO frequency cannot be controlled in such a way that the downconverted signal falls completely into the RX filter window. The proposed algorithms take care of this issue and can be used both in up- and in downstream reception.

Fig. 4 shows three different DSP schemes compared in this work whereas sketches of the signal spectra at different positions along the DSP chains are depicted in Fig. 5. While Fig. 4(a) illustrates the reference scheme which is denoted as *DSP Scheme-I* in the following, Fig. 4(b) and (c) illustrate two newly proposed schemes which are denoted as *DSP Scheme-II* and *DSP Scheme-III*, respectively. In all three schemes, the received signal is detected with an integrated coherent receiver (ICR) having 4 real-valued electrical outputs ($\underline{r}_{x'',y''}(t)$ for US and $\underline{r}_{x',y'}(t)$ for DS) for I and Q in two polarizations, see (9) and (14). An

important difference between the schemes is that while *DSP Scheme-I* and *DSP Scheme-II* require a single-sided electrical receiver bandwidth of $\Delta f_{RX} \geq \Delta f_{FSR}$, *DSP Scheme-III* requires only half that bandwidth. The received electrical signals are sampled and quantized in 4 analog-to-digital converters (ADCs) with a sampling rate of $f_{Sa} = 2\Delta f_{RX}$.

In all three schemes, as the first step after analog-to-digital conversion, we apply front-end corrections to compensate for possible imbalances, skews, and offsets between the four receiver outputs. The real and imaginary parts in each received polarization are then combined to form a complex-valued number as indicated by the double-line arrows in Fig. 4 at points Ⓐ and Ⓑ, respectively.

As pointed out earlier, we allow the emission frequency of a DFB laser to vary within a broad range due to temperature changes and manufacturing tolerances. This implies that the frequency offset between the DFB laser and the closest line of the frequency comb source in the OLT is different for each ONU. In upstream operation, the received spectra can therefore be positioned anywhere within the range of the LO frequency comb. Similarly, in downstream operation, the LO in the ONU can be positioned anywhere within the modulated frequency comb spectrum. Dependent on the available receiver bandwidth, we propose either *DSP Scheme-II* or *DSP Scheme-III* in order to optimize the system performance. In Fig. 5(a), (b), and (c), we consider the following three cases:

1) *Reference case without any receiver-bandwidth limitation:* The reference power spectrum after ideal balanced detection and front-end correction includes one copy of the signal spectrum per comb line as sketched in Fig. 5(a). The dash-dotted yellow and dotted orange lines represent low- and high-bandwidth receive filters, respectively. The intermediate frequency in US is $\Delta f_{IF}^{(i)\uparrow} = \min \left| f_L^{(i)} - (f_{LO} + n\Delta f_{FSR}) \right|$, and in DS we have $\Delta f_{IF}^{(i)\downarrow} = \min \left| (f_L + n\Delta f_{FSR}) - f_{LO}^{(i)} \right|$. If the frequency offset is referred to as $\Delta f_{IF}^{(i)}$ only, it has to be properly interpreted as either $\Delta f_{IF}^{(i)\uparrow}$ or $\Delta f_{IF}^{(i)\downarrow}$.

2) *Receiver bandwidth $\Delta f_{FSR} \leq \Delta f_{RX}$:* The received spectrum contains at least one full copy of the data spectrum and usually partial copies towards higher and lower frequencies, depending on the frequency of the DFB laser with respect to the comb source frequency. From now on, we refer to this receiver as the *high-bandwidth receiver* (HBW-RX). An exemplary power spectrum at point Ⓐ in Fig. 4(a) and (b) with a frequency offset of Δf_{IF} is sketched in Fig. 5(b), where the roll-off of the spectrum results from the receiver bandwidth limitation. In this example, the RX bandwidth equals the FSR, $\Delta f_{RX} = \Delta f_{FSR}$. Only in the special case, where the emission frequency of the ONU laser is located exactly in the middle of two comb lines, two full copies of the signal spectrum are received.

3) *Receiver bandwidth $\frac{1}{2}\Delta f_{FSR} \leq \Delta f_{RX} < \Delta f_{FSR}$:* Two partial copies of the signal spectrum are received unless the emission frequency of the DFB laser exactly matches a comb line. From now on, we refer to this receiver as the *limited-bandwidth receiver* (LBW-RX). An exemplary power spectrum at point Ⓑ in Fig. 4(c) with
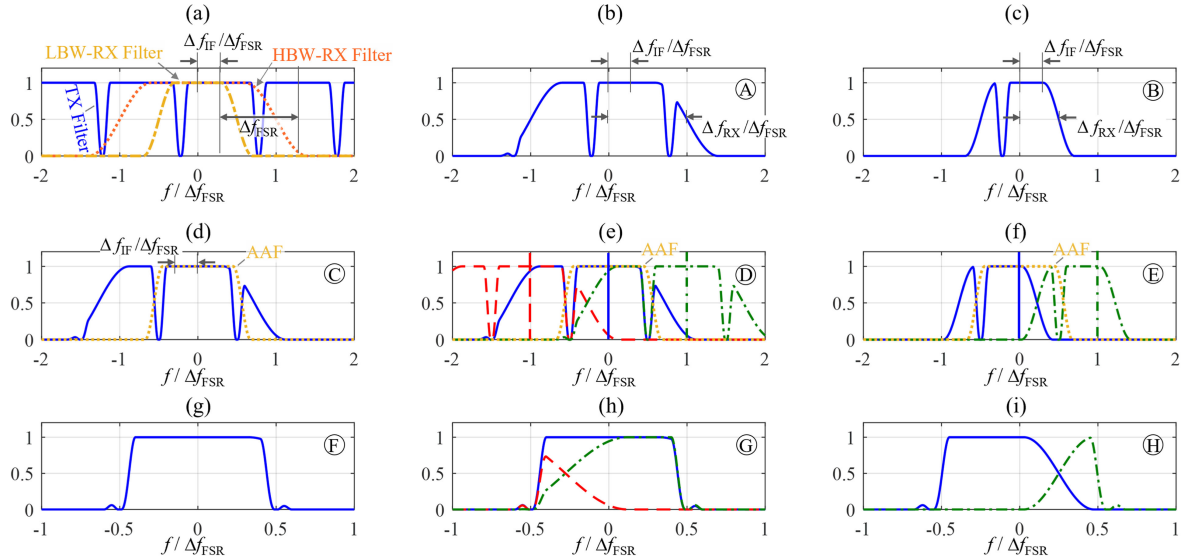
Fig. 5. Schematic representations of baseband signal spectra at different positions along the three different DSP schemes in Fig. 4, indicated by encircled capital letters (Ⓐ–Ⓗ). In the present example, the symbol rate is set to $f_{\text{Sym}} = (8/9) \times \Delta f_{\text{FSR}}$ for avoiding spectral overlap caused by finite TX filter slopes. (a) Reference signal spectrum after ideal balanced detection if the receiver bandwidth is infinitely large. The TX filter slopes are clearly to be seen. The frequency offset is set to $(5/16) \times f_{\text{Sym}}$. The dash-dotted yellow and dotted orange lines represent low- and high-bandwidth receive filters, respectively. (b) Signal spectrum if the one-sided half-power bandwidth of the receiver filter equals the FSR ($\Delta f_{\text{RX}} = \Delta f_{\text{FSR}}$). In this case, we receive a full copy of the data spectrum, and a partial copy of the spectra at either side. (c) Signal spectrum if the bandwidth of the receiver filter equals half the FSR ($\Delta f_{\text{RX}} = \frac{1}{2}\Delta f_{\text{FSR}}$). In this case, only (two) partial copies of the data spectrum are received. (d) Power spectrum after coarse frequency offset estimation (CFOC) in case of $\Delta f_{\text{RX}} = \Delta f_{\text{FSR}}$. The dotted yellow line represents anti-aliasing filter (AAF). (e) Power spectra after Signal Tripling & Spectral Sifting in case of $\Delta f_{\text{RX}} = \Delta f_{\text{FSR}}$. The signal after CFOC is colored in blue, whereas its copies shifted by $-\Delta f_{\text{FSR}}$ and $+\Delta f_{\text{FSR}}$ after CFOC are highlighted in red (dashed) and green (dash-dotted), respectively. The dotted yellow line represents AAF. (f) Power spectra after CFOC and Signal Doubling & Spectral Sifting in case of $\Delta f_{\text{RX}} = \frac{1}{2}\Delta f_{\text{FSR}}$. The dotted yellow line represents AAF. (g) Power spectrum after AAF in case of *DSP Scheme-I*. (h) Power spectrum after AAF in the case of *DSP Scheme-II*. The MIMO equalizer combines coherently the blue, the red, and the green signals and hence improves the SNR. (i) Power spectrum after AAF in case of *DSP Scheme-III*. Note that for sub-figures (g-i) the horizontal scale doubles.

a frequency offset of Δf_{IF} is shown in Fig. 5(c). In this example, the RX bandwidth equals half the FSR, $\Delta f_{\text{RX}} = \frac{1}{2}\Delta f_{\text{FSR}}$.

In the DSP block following positions Ⓐ and Ⓑ, we employ a coarse frequency offset compensation (CFOC) for reducing the frequency offset to a value that can be handled by the subsequent carrier recovery. The CFOC algorithm works as follows: First, we apply a fast Fourier transform (FFT) with a size of 1024 to the time sequence delivered by the previous DSP block. Then we identify the spectral dips (for HBW-RX) or dip (for LBW-RX), which are visible as long as the signal shaping TX filter with bandwidth Δf_{TX} is designed with a sufficiently sharp roll-off. For the HBW-RX, Fig. 5(b), the center frequency between these two dips defines the frequency offset $\Delta f_{\text{IF}}^{(i)}$. For the LBW-RX, Fig. 5(c), we observe a dip at f_{dip} within the frequency range $-\Delta f_{\text{RX}} < f_{\text{dip}} < +\Delta f_{\text{RX}}$, from which we identify the frequency offset $\Delta f_{\text{IF}}^{(i)} = f_{\text{dip}} + \frac{1}{2}\Delta f_{\text{FSR}}$, for $f_{\text{dip}} < 0$, and $\Delta f_{\text{IF}}^{(i)} = f_{\text{dip}} - \frac{1}{2}\Delta f_{\text{FSR}}$, for $f_{\text{dip}} \geq 0$. A sketch of the shifted signal spectrum from Fig. 5(b) at the output of the CFOC at point Ⓒ in Fig. 4(a) is shown in Fig. 5(d). The blue power spectra of Fig. 5(e) and (f) represent the CFOC outputs for *DSP Scheme-II* and *DSP Scheme-III* in Fig. 4(b) and (c), respectively. Chromatic dispersion (CD) compensation can be applied either before or after the CFOC block.

In the following, we discriminate between the three schemes shown in Fig. 4. While *DSP Scheme-I* follows the steps of a conventional digital coherent receiver, it requires a HBW-RX.

With *DSP Scheme-II*, we introduce an advanced DSP technique, which makes use of all copies of the received signal spectrum. As a result, it improves the signal-to-noise ratio (SNR). Finally, with *DSP Scheme-III*, we introduce another advanced DSP scheme, which features the use of a LBW-RX.

A. DSP Scheme-I (With 2 × 2 MIMO)

For this scheme, we restrict the processing to the case illustrated in Fig. 5(d), where a full copy of the data spectrum is received by a HBW-RX. It requires an ADC with an analog bandwidth exceeding the FSR (Δf_{FSR}), i.e., its sampling rate f_{Sa} must exceed $2\Delta f_{\text{RX}}$.

We first remove the redundant partial copies by employing an anti-aliasing filter (AAF) in combination with downsampling to two samples per I and Q symbol after the coarse frequency-offset compensation. In this work, we choose an AAF with a root-raised-cosine (RRC) shaped frequency response and a roll-off factor of 0.02, independently of the TX filter shape. Other filter shapes could be used as well. Fig. 5(g) illustrates the power spectrum after the AAF at point Ⓕ in Fig. 4(a). Next, we apply a frequency-domain feed-forward timing recovery (TR). More specifically, we estimate the timing error by employing a frequency-domain algorithm proposed by Barton & Al-Jalili, and compensate the timing error by a seventh-order Lagrange interpolation [41], [42]. Afterwards, we use a 2 × 2 MIMO adaptive equalizer whose coefficients are adapted by the constant modulus algorithm (CMA) [43] to correct for the

polarization rotation, to compensate for residual CD, and to mitigate the effect of bandwidth limitations as well as multipath and intersymbol interference in the transceivers [44]. Finally, we apply a carrier recovery (CR) [45] to compensate for the residual frequency offset as well as for laser phase noise using the Viterbi-Viterbi algorithm. We finalize the DSP by demapping and decoding.

B. DSP Scheme-II (With 6 × 2 MIMO)

In order to utilize all copies of the received signal spectrum, we introduce advanced *DSP Scheme-II* based on signal tripling, spectral shifting and 6 × 2 MIMO equalizer, see Figs. 4(b) and 5(b), (e), and (h). In the first step, we digitally create two copies of the dual-polarization received signal. Next, we simultaneously process this signals in three DSP lanes, namely "blue-lane," "green-lane," and "red-lane". The "blue-lane" operates on original signal delivered by CFOC and the corresponding power spectrum is shown in blue solid line in Fig. 5(e). The adjacent "green-lane" and "red-lane" operate on the digitally create copies, whose spectra are shifted to the right and to the left by $\pm\Delta f_{\text{FSR}}$, respectively. Spectral shifting requires an FSR detection algorithm. Fig. 5(e) illustrates the shifted signal spectra of the "green-lane" and the "red-lane" in green dash-dotted line and in red dashed line, respectively. Next, we apply the same AAF to all three lanes, cutting away unnecessary spectral parts as seen in Fig. 5(h). After downsampling and timing recovery as described in Subsection IV-A, a MIMO equalizer adds up the various lanes coherently: The addition of the "red-lane" and the "green-lane" outputs result in an identical signal as delivered by the "blue-lane," and adding all three lane outputs coherently therefore results in a 2-fold increase of the signal amplitude. In case the noise is uncorrelated, this increases the signal-to-noise ratio (SNR) by a factor of two. However, this requires a receiver with twice the bandwidth.

Each lane processes two polarizations, therefore the 2 × 2 MIMO equalizer of Fig. 4(a) has to be extended to a 6×2 MIMO equalizer in Fig. 4(b), which acts as an adaptive maximum ratio combiner [46]. As in *DSP Scheme-I*, the MIMO equalizer also corrects for the polarization rotation and the CD. Finally, the CR algorithm is applied. Notice that the proposed 6 × 2 MIMO equalizer will only converge if the phase difference $\Delta\phi_{\text{L,LO}}^{(n)}$ ((4) for DS and (13) for US) between neighboring comb lines is only slowly varying in comparison to the symbol rate Δf_{Sym}. Therefore, a coherent frequency comb source, as defined in Subsection III-A4, is required.

C. DSP Scheme-III (With 4 × 2 MIMO)

DSP Scheme-III allows to use intradyne coherent receivers with a minimum bandwidth. The principle is much the same as described in Section IV-B, however, only two processing lanes are employed: A digital copy of the data spectrum is created and shifted by either $+\Delta f_{\text{FSR}}$ or $-\Delta f_{\text{FSR}}$. Fig. 5(f) shows an exemplary power spectrum at point Ⓔ in Fig. 4(c). The sign of this frequency shift is chosen according to the direction of the frequency offset: The spectrum is moved in positive direction for positive frequency offsets, and in negative direction if the
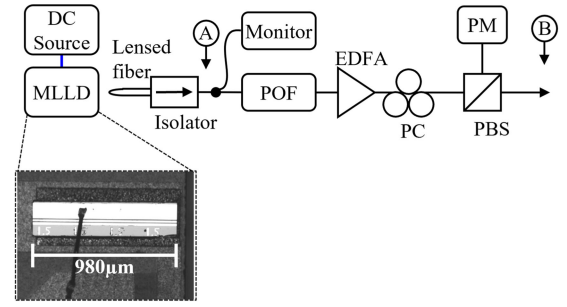

Fig. 6. Experimental setup of the coherent frequency comb source. A microscope image of the 980-μm-long quantum-dash mode-locked laser diode (MLLD) is shown in the inset [47]. Notice that only a DC current is supplied through the wire bond. The light generated by the MLLD is coupled into a lensed optical fiber. The optical isolator avoids back reflection into the MLLD. We use a programmable optical filter (POF) followed by an EDFA to amplify the signal and to equalize the comb lines at position Ⓑ. A polarization controller (PC), a polarization beam splitter (PBS), and a power meter (PM) are used to align the polarization across all comb lines. Point Ⓑ is connected with the DP-IQM (downstream) or the CRX (upstream).

frequency offset is negative. The subsequent DSP blocks are identical to the ones used in *DSP Scheme-II*, with the exception that only a 4 × 2 MIMO equalizer is needed. Fig. 5(i), shows the power spectrum after the AAF at point Ⓗ in Fig. 4(c). While a detailed analysis of the DSP power consumption is outside the scope of this paper, we would like to point out that we do not expect a significant increase, especially for *DSP scheme-III*, since most of the DSP functionalities remain unchanged.

V. EXPERIMENTAL SETUPS

In order to investigate the feasibility of the proposed colorless coherent TDM-PON architecture, we set up two experiments, one for downstream operation and another one for upstream operation. There are several options for frequency comb laser sources, such as Erbium glass oscillator (ERGO) lasers, electro-optic modulators, Kerr microresonators, and mode-locked laser diodes (MLLD). In our experiment, we use an MLLD as a frequency comb source. Fig. 6 shows the experimental setup for generating a flat-top coherent frequency comb. The MLLD is 980 μm long. Its light is outcoupled by a lensed fiber. With the help of integrated optics, a more stable and accurate coupling can be realized by using 3D printed waveguides or free-form coupling elements for hybrid photonic or flip-chip coupling technology [48]–[50]. Next, we employ an optical isolator to avoid back reflections into the MLLD. At room temperature and with a DC current of 180mA, we measure an optical power of +5dBm at position Ⓐ in Fig. 6. Fig. 7(a) shows the power spectrum measured at position Ⓐ in Fig. 6. The measured 3 dB bandwidth is 1.42 THz and the FSR is 25.0812 GHz at room temperature with a DC current of 180 mA. Note that we do not utilize any temperature controller to stabilize the output signal of the MLLD in our experiment. As a monitor we employ an optical power meter (PM) and a 43 GHz photodiode followed by an electrical spectrum analyzer (ESA). The ESA allows to measure the RF beat signal of the comb lines. The generated frequency comb is spectrally flattened with a programmable
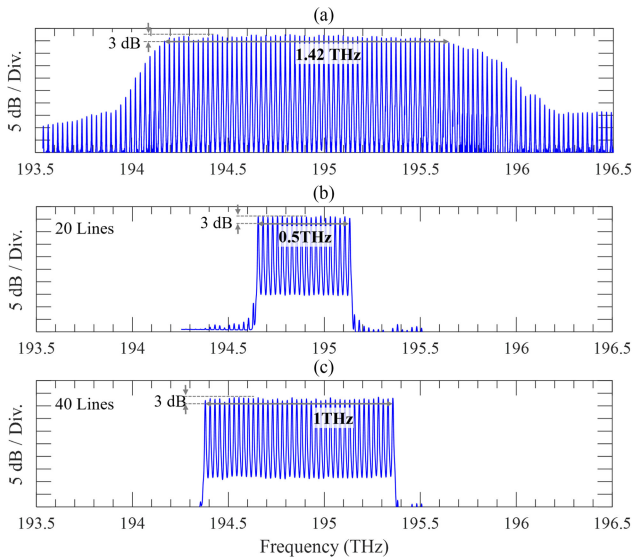
Fig. 7. Optical spectra of the frequency comb source measured in a resolution bandwidth of 2 GHz. (a) Optical spectrum measured at position Ⓐ in Fig. 6 for a DC current of 180 mA. We find a 3-dB bandwidth of 1.4 THz and an FSR of 25.0812 GHz. The optical power coupled into the lensed-fiber is 5 dBm. (b) Optical spectrum measured at position Ⓑ in Fig. 6. With the POF we filtered out 20 comb lines and equalized them to within about $\pm$ 0.5 dB. (c) Corresponding optical spectrum for 40 comb lines.
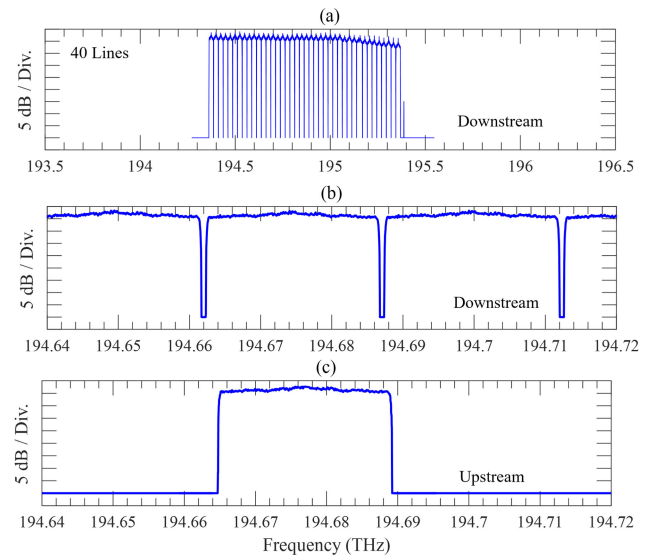

Fig. 8. Modulated optical spectra for both US and DS operation. (a) Optical comb spectrum modulated with a 24-GBd QPSK signal, spectrally shaped with a root-raised-cosine (RRC) filter having a roll-off of 0.02, measured at position Ⓑ in Fig. 2. Towards higher frequencies, we observe the effect of a reduced gain of the EDFA following the modulator. (b) Same as (a) but plotted over a narrower frequency range. (c) Optical spectrum of the modulated output of a DFB laser centered at 194.68 THz measured at position B in Fig 3. The resolution bandwidth is 180 MHz in all measurements shown in the figure.

optical filter (POF, Finisar waveshaper 4000 s) and reduced to a desired number of comb lines, which are then amplified with an EDFA. With the polarization controller (PC) and a polarization beam splitter (PBS) we set the correct polarization state so that we can efficiently couple into the polarization maintaining fiber. Fig. 7(b) and (c) shows the flattened comb spectrum of 20 and 40 lines at position Ⓑ in Fig. 6, respectively. As can be seen in the figure, the peak power variation is about $\pm$ 0.5 dB in both cases, except for a single comb line in case of 40 lines in Fig. 7(c). Note that 20 and 40 lines correspond to bandwidths of 0.5 THz and 1.0 THz, respectively. The measured output power of the spectrally flattened comb at position Ⓑ in Fig. 6 is +16 dBm for all cases. Next, we modulate all comb lines with a LiNbO$_3$ DP-IQM, driven by a four-channel arbitrary-waveform generator (AWG, 120 GSa/s, Keysight M8194 A). The test patterns consist of two uncorrelated pseudo random sequences of 2^{15} QPSK symbols, which are over-sampled, and then shaped by a pulse-shaping filter exhibiting a RRC spectrum. The FSR of the coherent frequency comb generated with the MLLD is 25.0812 GHz and limits the symbol rate to 24 GBd when considering a sharp roll-off of 0.02 for the RRC pulse shaping. With a frequency comb with slightly higher FSR, symbol rate can easily be scaled to 25 GBd, resulting in a bit rate of 100 Gbit/s. In the downstream case, the modulated signal is amplified with a booster EDFA, resulting in the comb spectrum depicted in Fig. 8(a) measured at position Ⓑ of Fig. 2. We attribute the power drop at high frequencies to a gain tilt of the EDFA. Fig. 8(b) provides a closer look into the modulated spectrum.

In an optical back-to-back setting, we vary the received power with a variable optical attenuator (VOA). For our fiber nonlinearities experiment, we employ 25 km of standard

single-mode fiber (SSMF) that along with the VOA emulates the ODN. In that case, the launch power into the fiber is controlled by a concatenation of two booster amplifiers (instead of only one in optical back-to-back) followed by another VOA. At the ONU side, we receive the optical signal with an integrated coherent receiver (ICR, Neophotonics, OIF Type II). The ICR features a bandwidth of more than 25 GHz, which is larger than the FSR (HBW-RX, compare Subsection IV-A and IV-B). Thus, we have to emulate the case of an LBW-RX (Subsection IV-C) by applying a digital low-pass filter with a bandwidth of 13 GHz and a roll-off of 0.3 at the beginning of our DSP chain. In addition, due to a limited number of available devices in our laboratory, we set up only one ONU transmitter and receiver. However, we mimic different ONUs by sweeping the ONU laser frequency. We use a 3 dB power splitter and a power meter to measure the received optical power impinging on the coherent receiver. In our experiments, we measure the receiver sensitivity for two different types of LOs, one being a DFB laser emitting at ~194.68 THz (~1540.00 nm) and the other being a narrow-linewidth tunable ECL. Our setup allows us to tune the ONU LO frequency over the full bandwidth of the frequency comb (1.05 THz) even if 40 lines are used.

For upstream, the experimental setup is modified as follows: The DFB laser, or alternatively the ECL, is used as the transmit laser at the ONU side, whereas the same DP-IQM as for the downstream is used. The measured upstream signal at position Ⓑ of Fig. 3 for an exemplary ONU laser frequency of ~194.68 THz is shown in Fig. 8(c). The received optical signal is pre-amplified using an EDFA at the OLT side. Note that we do not employ an optical filter for removing out-of-band ASE noise, since we want to demonstrate a wide variation of the ONU
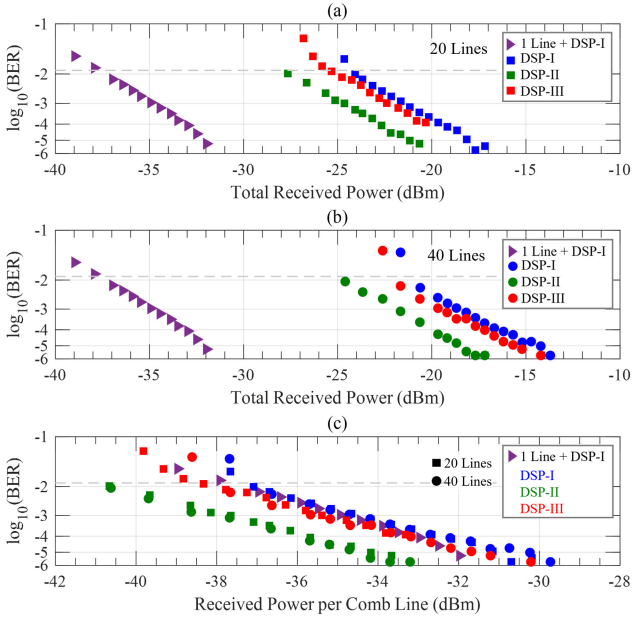
Fig. 9. Downstream operation. Measured BER for the three DSP schemes shown in Fig. 4. Here, blue, green, and red colors represent values obtained with *DSP schemes I, II* and *III*, respectively. As a reference, purple triangles represent the values for a single-line ECL and the DSP scheme I. The BER is plotted as a function of the total optical power received at the ONU for (a) 20 comb lines, and for (b) 40 comb lines. The LO is a DFB laser for all measurements. (c) BER from (a) and (b) plotted as a function of the received optical power per comb line.

wavelengths. The frequency comb generated by the MLLD acts as an LO and allows the ONU laser frequency to drift over the entire comb. For reception, we use the same ICR as for the downstream.

In both experiments, we use a four-channel real-time oscilloscope with a sampling rate of 256 GSa/s and a realtime bandwidth of 80 GHz to capture the outputs of the ICRs. Afterwards, offline digital-signal processing algorithms are applied to the recorded waveforms, see Section IV for details. As a final step, the bit error ratio (BER) is estimated by evaluating 2^{19} bit.

VI. EXPERIMENTAL RESULTS

A. Downstream Colorless Coherent PON

First, we investigate the downstream operation in a back-to-back configuration. As described before, see Section III-B and Fig. 2, a frequency comb generated by an MLLD is used as the transmit laser at the OLT, whereas the LO at the ONU is provided by a DFB laser. At the transmitter, we use the POF to select 20 or 40, respectively. The output power of the booster EDFA is set to a constant value of 8 dBm. As a result, the transmit power per line is reduced by a factor of 20 if 20 comb lines are considered and by a factor of 40 if 40 comb lines are used. The received optical power is swept by tuning a VOA.

In a first experiment, we characterize the ONU receiver. To this end, we measure the BER when sweeping the total received power (including all transmitted comb lines) by tuning a VOA, see in Fig. 9. The blue, green and red colors represent the BER obtained with *DSP Scheme-I*, *DSP Scheme-II* and *DSP*

Scheme-III, respectively. Furthermore, the square and the circle symbols illustrate the BER for 20 comb lines (see Fig. 9(a) and (c)) and for 40 comb lines (see Fig. 9(b) and (c)). As a reference, we also measure the BER by using a single ECL as transmitter laser, see purple triangles in Fig. 9. The evaluation is first done with *DSP Scheme-I* employing a 2×2 MIMO equalizer, see blue symbols in Fig. 9(a) and (b). Considering a BER threshold of 1.25×10^{-2} for a forward error correction (FEC) code with 15% overhead [51], we observe receiver sensitivities of (leading to loss budgets of) -38 dBm (46 dB), -24.5 dBm (32.5 dB), and -21.5 dBm (29.5 dB) for the case of a single ECL, for 20 comb lines, and for 40 comb lines used in the OLT transmit laser, respectively. When replacing the DFB laser used as LO at the ONU by a low-linewidth ECL and when repeating the same experiment, we do not observe a substantial performance degradation. This indicates that phase noise is none of the dominant system limitations, because the linewidth of the DFB laser is already sufficiently low.

Next we evaluate the measured data with our proposed DSP schemes (*DSP Scheme-II*), and compare the results with the conventional procedure (*DSP Scheme-I*). The outcome is depicted with green symbols in Fig. 9(a) and (b). This time, we restrict our investigation to the case of a DFB laser as an LO, but again compare two different transmitter scenarios: 20 comb lines (Fig. 9(a)), and 40 comb lines (Fig. 9(b)). In both cases, we observe a 3 dB improvement of the receiver sensitivity and of the loss budget when replacing *DSP Scheme-I* by *DSP Scheme-II* for an HBW-RX. This improvement results from an SNR increase by 3 dB, when using the energy contained in the partial copies of the received spectrum, see Section IV-B.

We then assume an LBW-RX ($\frac{1}{2}\Delta f_{FSR} \leq \Delta f_{RX} < \Delta f_{FSR}$) and repeat our evaluation (with *DSP Scheme-III*). For this purpose, we apply a digital low-pass filter and artificially reduce the double-sided bandwidth of our receiver to 13 GHz. Comparing the receiver sensitivity obtained for *DSP Scheme-I* with the one achieved by processing according to *DSP Scheme-III*, we find a performance improvement of 0.5 dB (see red symbols in Fig. 9(a) and (b)). We attribute this gain to the extra signal power that is contained in the additional partial copy of the data spectrum ($\Delta f_{RX} > \Delta f_{TX}$) which is taken into account when applying the 4×2 MIMO equalizer, see Section IV-C.

The results presented so far show that the receiver sensitivity scales in proportion to the number of comb lines. This becomes even more visible in Fig. 9(c), where the BER for 20 and 40 comb lines as a function of the received power per comb line nicely coincide. The BER obtained with a single-line ECL transmitter laser is again plotted for comparison.

As described in Section II, our proposed colorless coherent TDM-PON architecture aims at solving the challenge of matching the transmitter frequency with the corresponding receiver LO frequency. To demonstrate that we can cope with substantial manufacturing tolerances and temperature-induced wavelength drifts of the DFB lasers used in the ONUs, we investigate the system performance when tuning the LO frequency over the full bandwidth of the comb spectrum. Since DFB lasers are not tunable over frequency ranges in the order of 1 THz and a large enough sample of differently emitting DFB lasers was
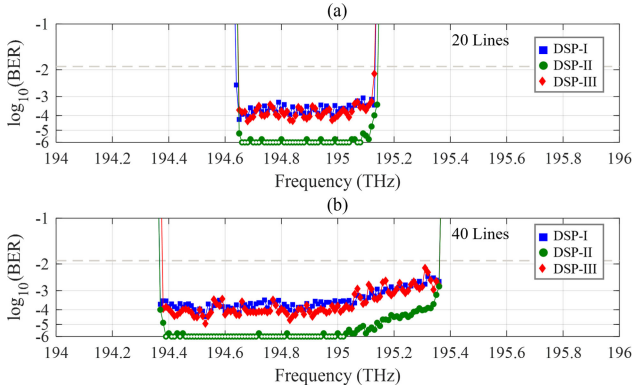
Fig. 10. BERs measured when the LO generated by an ECL is swept over frequency for (a) 20 and (b) 40 comb lines, corresponding to an LO frequency (wavelength) variation of ± 0.25 THz (± 2 nm) or ± 0.5 THz (± 4 nm), respectively. The open symbols indicate that no bit errors.
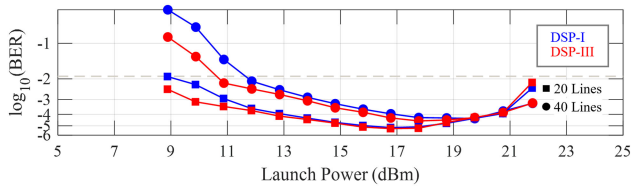

Fig. 11. BER as a function of the launch power into a 25 km SSMF followed by 25 dB additional ODN loss. The circled and squared symbols represent the transmit laser consisting of 20 and 40 comb lines, respectively. A DFB laser is used as a LO. The blue color represents *DSP Scheme-I* and the red color represents *DSP Scheme-III*.

Fig. 12. Upstream operation. Measured BERs for the three DSP schemes shown in Fig. 4. Blue, green and red colors represent *DSP schemes I*, *II*, and *III*, respectively. Purple triangles represent the back-to-back measurement using an ECL LO and conventional coherent DSP. The BER is plotted as a function of the total optical power received at the OLT for (a) 20 comb lines, and (b) 40 comb lines. (c) BER plotted as a function of the received optical power per LO comb line considering 20 and 40 comb lines.

not available, we employed a tunable ECL as an LO. This choice reflects real-world BER results because we already showed the equivalence of ECL and DFB laser as an LO. The results of our experiments are summarized in Fig. 10 for a received power of -20 dBm in the case of 20 comb lines (Fig. 10(a)), and a received power of -17 dBm in the case of 40 comb lines (Fig. 10(b)). As before, the blue, the green, and the red color represent *DSP Scheme-I*, *II*, and *III*. Open symbols indicate that no errors could be detected in the recorded data. For all cases, we measure a BER that is below the 15 % FEC limit. The slight increase of the BER towards higher frequencies, Fig. 10(b), is caused by a gain tilt of the booster amplifier. The experimental results confirm that our TDM-PON architecture can tolerate LO frequency (wavelength) variations at the ONU of ± 0.25 THz (± 2 nm) if 20 comb lines are used and ± 0.5 THz (± 4 nm) if 40 comb lines are used.

Finally, we investigate the proposed architecture in the presence of fiber nonlinearities. To this end, we slightly modify the experimental setup. We insert 25 km of standard single-mode fiber (SSMF) and set the subsequent VOA to a constant attenuation of 25 dB to emulate the loss of the passive splitter. This leads to an accumulated loss of about 30 dB, which is a typical number for ODN losses in PONs. To control the launch power going into the SSMF, we deploy a second booster EDFA and another VOA in front of the fiber. We measure the BER for various launch powers to find the optimum operating point of the system, see Fig. 11. The optimum launch power is 17 dBm
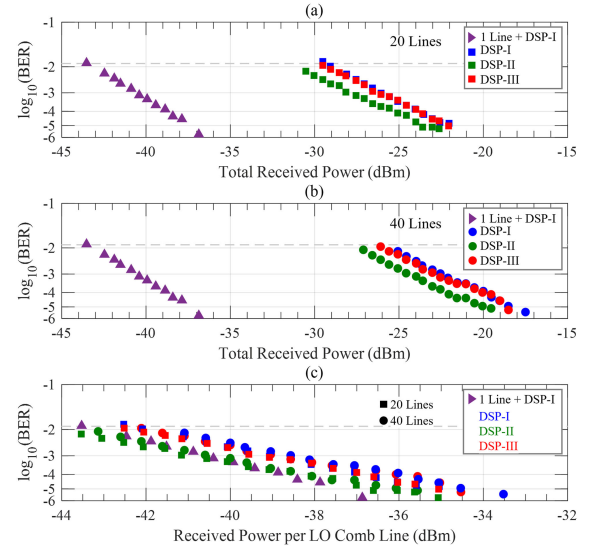
and 20 dBm for 20 comb lines and 40 comb lines, respectively. The 3 dB difference is due to the 3 dB reduction of the launch power per comb line in the case of 40 comb lines.

B. Upstream Colorless Coherent PON

For upstream operation, we first investigate the receiver sensitivities. For the evaluation of the received data, we use *DSP Scheme-I* with a 2×2 MIMO equalizer. According to Section IV-A and Fig. 3, a DFB laser is used as the transmit laser in the ONU, while a frequency comb acts as the LO in the OLT. Similar to downstream operation, the received power is swept by tuning a VOA. We select either 20 or 40 comb lines for the LO and compare the system performance for both cases, see Fig. 12(a) and (b). We plot the BER as a function of the received power measured at the input of the OLT pre-amplifier. The total LO power is kept constant at 16 dBm so that the LO power per comb line decreases with an increasing number of lines used. As a reference, we also measure the BER for a single-line ECL as an LO, see purple labels in Fig. 12.

Furthermore, we repeat the measurements when replacing the DFB transmit laser by an ECL and observe an improvement by 0.5 dB, which we attribute the carrier-to-noise power ratio (OCNR) which is better by 0.5 dB compared to the DFB laser. For the DFB as a transmit laser, we find receiver sensitivities of -43.5 dBm (ECL as LO), -29.5 dBm (20 LO comb lines), and -26 dBm (40 LO comb lines) at the 15 % FEC limit (see Fig. 12(a) and (b)). The differences mainly result from the reduction of the power per LO laser line by a factor of 20 (40) if 20 (40) comb lines are used as LO. We attribute the additional penalty of 1 dB to a reduced OCNR and accumulated LO-ASE beat noise, see Section III-C. Finally, we confirm a negligible
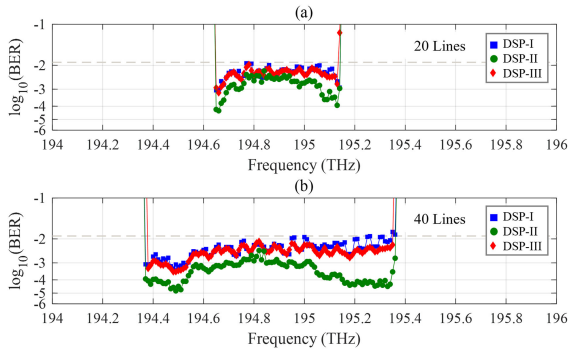
Fig. 13. BER obtained while tuning the center frequency of the ONU transmit laser and using either (a) 20 or (b) 40 comb lines as LO. These two cases mimic a transmit laser frequency variation of ± 0.25 THz (± 2 nm) and ± 0.5 THz (± 4 nm), which can occur due to fabrication constraints and temperature drift.

BER penalty in comparison with ECL and 1 line MLLD LO and conclude that the laser phase noise is sufficiently low.

In another evaluation, we again compare the proposed DSP schemes (*DSP Scheme-II and III*) with the conventional DSP processing (*DSP Scheme-I*). The results are depicted in Fig. 12. As for the downstream operation, we restrict our BER analysis to the case of a DFB laser at the ONU, but compare the results for an LO with 20 lines (Fig. 12(a)), and with 40 lines (Fig. 12(b)). Moreover, the BER achieved for an LO consisting of a single ECL line is plotted in purple triangles as a reference. The blue, green and red symbols correspond to *DSP Scheme-I, II*, and *III*, respectively. For an HBW-RX, we observe a substantial performance improvement when employing *DSP Scheme-II*. We find an improvement of 2.5 dB for 20 comb lines (see green square symbols in Fig. 12(a)), and an additional improvements of 2.0 dB for 40 comb lines (see green circle symbols in Fig. 12(b)). Compared to downstream operation, the improvement is less because of (partially) coherent LO-ASE beat noise within the neighboring signal bands (compare Fig. 9(a) and (b) with Fig. 12(a) and (b)). For the LBW-RX emulated by digital low-pass filtering of the ICR output signal, we find the same 0.5 dB receiver sensitivity gain as for downstream, when replacing *DSP Scheme-I* by *DSP Scheme-III* (see red symbols in Fig. 12(a) and (b)). As explained before, this improvement results from the additional signal power that is contained in the received spectrum and that can be extracted with *DSP Scheme-III*, but not by the conventional 2×2 MIMO processing.

In Fig. 12(c), we plot the measurement results as a function of the received power per LO comb line. The results indicate a negligible penalty of 1 dB compared to using a single ECL line as an LO. The penalty is increasing for higher received powers. This penalty is again caused by accumulated LO-ASE beat noise.

Finally, we emulate the wavelength variation of the ONU laser by tuning an ECL over the full bandwidth of the LO comb. As only a slight performance degradation (0.5 dB because of reduced OCNR) has been obtained with a DFB transmit laser compared to the ECL, we expect the results to be representative for a typical low-cost PON transmit laser. The results of the wavelength sweep are depicted in Fig. 13. For 20 (40) comb lines and at a received power of -28 dBm (-25 dBm), the BER

stays below the 15 % FEC limit over the entire comb bandwidth of 0.5 THz (1 THz). We attribute the variations in the BER largely to imperfect per-line power equalization of the LO and the gain tilt of the pre-amplifier EDFA.

In conclusion, we confirmed that the proposed colorless coherent TDM-PON architecture tolerates strong ONU lasers frequency (wavelength) variations even in the more challenging upstream scenario.

VII. Summary

Due to the growing amount of data traffic, it is to be expected that passive optical networks need to support data rates of 100 Gbit/s or more in the near future. Such high data rates can be achieved by employing DP-IQM and coherent receivers at the OLT as well as at the ONUs. On the one hand, coherent receivers require local oscillators that are precisely matched with the transmit lasers, which makes wavelength-stable and low-linewidth lasers the technology of choice. On the other hand, it is preferable to use low-cost DFB lasers in the ONUs because of the omnipresent economic constraints in access networks. DFB lasers in turn are subject to temperature-induced wavelength drifts and are manufactured in processes that can lead to significant wavelength variations of up to ± 4 nm from batch to batch. This dilemma is solved by our proposed colorless coherent TDM-PON architecture, which to the best of our knowledge is the first of its kind. It relies on a frequency comb laser at the OLT, which greatly relaxes the requirements for the wavelength accuracy and stability of the lasers in the ONUs. Furthermore, it avoids the need for LO wavelength matching between ONU and OLT lasers because the wavelength of the DFB lasers used in the ONUs can vary or drift within the entire comb bandwidth without causing a substantial performance penalty. We demonstrate error-free colorless coherent upstream and downstream operation over a wide bandwidth of 1 THz (± 4 nm) at an aggregated line rate of 96 Gbit/s. In addition, we report on an advanced DSP scheme based on Signal Tripling & Spectral Shifting after a coarse frequency offset compensation and a 6×2 MIMO equalizer. These measures improve the receiver sensitivity by 3 dB. Finally, we propose a DSP scheme based on a 4×2 MIMO equalizer, which works equally well for low-bandwidth receivers. We believe, that frequency comb laser sources have the potential to become a key building block in integrated burst-mode coherent receivers.

References

[1] X. Liu and F. Effenberger, "Emerging optical access network technologies for 5G wireless," *IEEE/OSA J. Opt. Commun. Netw.*, vol. 8, no. 12, pp. B 70–B79, Dec. 2016.

[2] B. Skubic, J. Chen, J. Ahmed, L. Wosinska, and B. Mukherjee, "A comparison of dynamic bandwidth allocation for EPON, GPON, and next-generation TDM PON," *IEEE Commun. Mag.*, vol. 47, no. 3, pp. S40–S48, Mar. 2009.

[3] J. S. Wey, "The outlook for PON standardization: A tutorial," *J. Lightw. Technol.*, vol. 38, no. 1, pp. 31–42, 2020.

[4] E. Harstead, D. van Veen, V. Houtsma, and P. Dom, "Technology roadmap for time-division multiplexed passive optical networks (TDM PONs)," *J. Lightw. Technol.*, vol. 37, no. 2, pp. 657–664, Jan. 2019.

[5] D. van Veen and V. Houtsma, "Strategies for economical next-generation 50G and 100G passive optical networks," *J. Opt. Commun. Netw.*, vol. 12, no. 1, pp. A95–A103, 2020.

[6] K. Hara *et al.*, "Flexible load balancing technique using dynamic wavelength bandwidth allocation (DWBA) toward 100 Gbit/s-class-WDM/TDM-PON," in *Proc. 36th Eur. Conf. Exhibit. Opt. Commun.*, Torino, Italy, 2010, Paper Tu.3.B–2.

[7] N. Suzuki, S. Yoshima, H. Miura, and K. Motoshima, "Demonstration of 100-Gb/s/λ-based coherent WDM-PON system using new AGC EDFA based upstream preamplifier and optically superimposed AMCC function," *J. Lightw. Technol.*, vol. 35, no. 8, pp. 1415–1421, Apr. 2017.

[8] Y. Luo *et al.*, "Time-and wavelength-division multiplexed passive optical network (TWDM-PON) for next-generation PON stage 2 (NG-PON2)," *J. Lightw. Technol.*, vol. 31, no. 4, pp. 587–593, Feb. 2013.

[9] D. Lavery, R. Maher, D. S. Millar, B. C. Thomsen, P. Bayvel, and S. J. Savory, "Digital coherent receivers for long-reach optical access networks," *J. Lightw. Technol.*, vol. 31, no. 4, pp. 609–620, Feb. 2013.

[10] M. S. Erkilinç *et al.*, "Polarization-insensitive single-balanced photodiode coherent receiver for long-reach WDM-PONs," *J. Lightw. Technol.*, vol. 34, no. 8, pp. 2034–2041, 2016.

[11] S. J. Savory, M. S. Faruk, and X. Li, "Low complexity coherent for access networks," in *Proc. Signal Process. Photon. Commun. Opt. Soc. Amer.*, 2020, Paper SpW 1I-3.

[12] Y. Zhu *et al.*, "Comparative study of cost-effective coherent and direct detection schemes for 100 Gb/s/λ PON," *J. Opt. Commun. Netw.*, vol. 12, no. 9, pp. D36–D47, 2020.

[13] M. S. Erkilinç *et al.*, "Comparison of low complexity coherent receivers for UDWDM-PONs (λ-to-the-user)," *J. Lightw. Technol.*, vol. 36, no. 16, pp. 3453–3464, 2018.

[14] N. Iiyama, J.-I. Kani, K.-I. Suzuki, and A. Ootaka, "Advanced DSP for optical access networks: Challenges and opportunities," in *Proc. Opt. Fiber Commun. Conf. Exhibit.*, San Francisco, CA, USA, 2015, Paper M3J.3.

[15] N. Iiyama, M. Fujiwara, T. Kanai, J.-I. Kani, and J. Terada, "The approaches of coherent technology for TDM-PON," in *Proc. Eur. Conf. Opt. Commun.*, Dublin, Ireland, 2019, pp. 1–3.

[16] J. Zhang *et al.*, "200 Gbit/s/λ PDM-PAM-4 PON system based on intensity modulation and coherent detection," *J. Opt. Commun. Netw.*, vol. 12, no. 1, pp. A1–A8, 2020.

[17] M. Erkilinç *et al.*, "PON transceiver technologies for ≥ 50 Gbits/s per λ: Alamouti coding and heterodyne detection," *J. Opt. Commun. Netw.*, vol. 12, no. 2, pp. A162–A170, 2020.

[18] J. Zhang, Z. Jia, M. Xu, H. Zhang, L. A. Campos, and C. Knittle, "High-performance preamble design and upstream burst mode detection in 100-Gb/s/λ TDM Coherent-PON," in *Proc. Opt. Fiber Commun. Conf.*, San-Diego, CA, USA, 2020, Paper W1E.1.

[19] D. van Veen and V. Houtsma, "Transceiver technologies for next-generation PON," in *Proc. Opt. Fiber Commun. Conf.*, San-Diego, CA, USA, 2020, Paper W1E.2.

[20] Q. Zhuge, "Cost-efficient architectures and signal processing for coherent PON systems," in *Proc Eur. Conf. Opt. Commun.*, Dublin, Ireland, 2019.

[21] S. Gudyriev *et al.*, "Coherent ePIC receiver for 64 GBaud QPSK in 0.25 μm photonic BiCMOS technology," *J. Lightw. Technol.*, vol. 37, no. 1, pp. 103–109, 2019.

[22] S. Lange *et al.*, "Low power InP-based monolithic DFB-laser IQ modulator with SiGe differential driver for 32-GBd QPSK modulation," *J. Lightw. Technol.*, vol. 34, no. 8, pp. 1678–1682, 2016.

[23] M. S. Faruk and S. J. Savory, "Coherent access: Status and opportunities," in *Proc. IEEE Photon. Soc. Summer Topicals Meeting Ser.*, 2020, pp. 1–2.

[24] Y. Kotaki, S. Ogita, M. Matsude, Y. Kuwahara, and H. Ishikawa, "Tunable, narrow-linewidth and high-power lambda/4-shifted DFB laser," *Electron. Lett.*, vol. 25, no. 15, pp. 990–992, 1989.

[25] G. Yoffe, S. Zou, S. Rishton, R. Olson, M. Emanuel, and B. Pezeshki, "Widely-tunable 30 mW laser source with sub-500 kHz linewidth using DFB array," in *Proc. IEEE 21st Annu. Meeting Lasers Electro- Opt. Soc.*, 2008, pp. 892–893.

[26] V. Sales, J. Segarra, V. Polo, J. C. Velásquez, and J. Prat, "UDWDM-PON using low-cost coherent transceivers with limited tunability and heuristic DWA," *IEEE/OSA J. Opt. Commun. Netw.*, vol. 8, no. 8, pp. 582–599, Aug. 2016.

[27] S. Sakano, T. Tsuchiya, M. Suzuki, S. Kitajima, and N. Chinone, "Tunable DFB laser with a striped thin-film heater," *IEEE Photon. Technol. Lett.*, vol. 4, no. 4, pp. 321–323, Apr. 1992.

[28] Z. Xu *et al.*, "High-speed WDM-PON using CW injection-locked fabry-pérot laser diodes," *Opt. Exp.*, vol. 15, no. 6, pp. 2953–2962, 2007.

[29] P. Healey *et al.*, "Spectral slicing WDM-PON using wavelength-seeded reflective SOAs," *Electron. Lett.*, vol. 37, no. 19, pp. 1181–1182, 2001.

[30] J. Simsarian and L. Zhang, "Wavelength locking a fast-switching tunable laser," *IEEE Photon. Technol. Lett.*, vol. 16, no. 7, pp. 1745–1747, Jul. 2004.

[31] J. E. Simsarian, J. Gripp, S. Chandrasekhar, and P. Mitchell, "Fast-tuning coherent burst-mode receiver for metropolitan networks," *IEEE Photon. Technol. Lett.*, vol. 26, no. 8, pp. 813–816, Apr. 2014.

[32] M. M. H. Adib *et al.*, "Colorless coherent passive optical network using a frequency comb local oscillator," in *Proc. Opt. Fiber Commun. Conf.*, San-Diego, CA, USA, 2019, Paper Th3F.4.

[33] M. M. H. Adib *et al.*, "24 GBd DP-QPSK upstream and downstream operation of a colourless coherent PON using an MLLD-based frequency comb," in *Proc. Eur. Conf. Opt. Commun.*, Dublin, Ireland, 2019, Paper M.1.F–2.

[34] X. Zeng *et al.*, "Frequency-offset-tolerant optical frequency comb-based coherent transmission for intra-datacenter interconnections," *Opt. Exp.*, vol. 29, no. 11, pp. 17522–17533, 2021.

[35] B. C. Thomsen, R. Maher, D. S. Millar, and S. J. Savory, "Burst mode receiver for 112 Gb/s DP-QPSK with parallel DSP," *Opt. Exp.*, vol. 19, no. 26, pp. B770–B776, 2011.

[36] R. Koma, M. Fujiwara, J. Kani, K. Suzuki, and A. Otaka, "Burst-mode digital signal processing that pre-calculates FIR filter coefficients for digital coherent PON upstream," *IEEE/OSA J. Opt. Commun. Netw.*, vol. 10, no. 5, pp. 461–470, May 2018.

[37] R. Koma, M. Fujiwara, J.-I. Kani, and T. Yoshida, "Fast feed-forward optical and electrical gain control to extend the dynamic range of the burst-mode digital coherent receiver for high-speed TDN-PON systems," *J. Lightw. Technol.*, vol. 40, no. 3, pp. 647–654, Feb. 2022.

[38] H. Rohde *et al.*, "Coherent ultra dense WDM technology for next generation optical metro and access networks," *J. Lightw. Technol.*, vol. 32, no. 10, pp. 2041–2052, 2014.

[39] S. Shibita, D. Hisano, K. Maruta, Y. Nakayama, K. Mishina, and A. Maruta, "Optical reflection interference equalization for single-wavelength bidirectional WDM-PON transmission system," *IEEE Photon. J.*, vol. 13, no. 1, pp. 1–15, Feb. 2021.

[40] M. Yamada, H. Ono, T. Kanamori, S. Sudo, and Y. Ohishi, "Broadband and gain-flattened amplifier composed of a 1.55 μm-band and a 1.58 μm-band Er3 -doped fibre amplifier in a parallel configuration," *Electron. Lett.*, vol. 33, no. 8, pp. 710–711, 1997.

[41] S. Barton and Y. Al-Jalili, "A symbol timing recovery scheme based on spectral redundancy," in *Proc. IEE Colloq. Adv. Modulation Coding Techn. Satell. Commun.*, 1992, pp. 1–6.

[42] P. Matalla, M. S. Mahmud, C. Füllner, C. Koos, W. Freude, and S. Randel, "Hardware comparison of feed-forward clock recovery algorithms for optical communications," in *Proc. IEEE Opt. Fiber Commun. Conf. Exhibit.*, 2021, Paper Th1A–10.

[43] D. Godard, "Self-recovering equalization and carrier tracking in two-dimensional data communication systems," *IEEE Trans. Commun.*, vol. 28, no. 11, pp. 1867–1875, Nov. 1980.

[44] S. J. Savory, "Digital filters for coherent optical receivers," *Opt. Exp.*, vol. 16, no. 2, pp. 804–817, 2008.

[45] A. Viterbi, "Nonlinear estimation of PSK-modulated carrier phase with application to burst digital transmission," *IEEE Trans. Inf. Theory*, vol. 29, no. 4, pp. 543–551, Jul. 1983.

[46] S. Song, K. Aizawa, and M. Hatori, "A blind adaptive array based on CMA and LMS," *Electron. Commun. Jpn. Part III Fundam. Electron. Sci.*, vol. 81, no. 7, pp. 37–44, 1998.

[47] G.-H. Duan *et al.*, "High performance InP-based quantum dash semiconductor mode-locked lasers for optical communications," *Bell Labs Tech. J.*, vol. 14, no. 3, pp. 63–84, 2009.

[48] S. Tanaka, S.-H. Jeong, S. Sekiguchi, T. Kurahashi, Y. Tanaka, and K. Morito, "High-output-power, single-wavelength silicon hybrid laser using precise flip-chip bonding technology," *Opt. Exp.*, vol. 20, no. 27, pp. 28057–28069, 2012.

[49] B. Song, C. Stagarescu, S. Ristic, A. Behfar, and J. Klamkin, "3D integrated hybrid silicon laser," *Opt. Exp.*, vol. 24, no. 10, pp. 10435–10444, 2016.

[50] P.-I. Dietrich *et al.*, "In situ 3D nanoprinting of free-form coupling elements for hybrid photonic integration," *Nature Photon.*, vol. 12, no. 4, pp. 241–247, 2018.

[51] B. Smith, I. Lyubomirsky, and S. Bhoja, "Leveraging 400G ZR FEC technology," in *Proc. IEEE 802.3 Beyond 10 km Opt. PHYs Study Group*, Orlando, FL, USA, 2017. [Online]. Available: http://www.ieee802.org/3/B10K/public/17_11/lyubomirsky_b10k_01_1117.pdf

Md Mosaddek Hossain Adib (Student Member, IEEE) received the master's degree in optics and photonics in 2017 from the Department of Electrical Engineering and Information Technology, Karlsruhe Institute of Technology (KIT), Karlsruhe, Germany, where he is currently working toward the Ph.D. degree in electrical engineering. Since 2017, he has been a Research Associate with the Institute of Photonics and Quantum Electronics, KIT. His research interests include the investigation of optical access network architectures and digital signal processing algorithms. Mr. Hossain was the recipient of the Best Student Paper Award (honorable mentions) at the OPTICA (formerly OSA) Advanced Photonics Congress 2020.

Christoph Füllner (Student Member, IEEE) received the B.S. and M.S. degrees in electrical engineering in 2014 and 2016, respectively, from the Karlsruhe Institute of Technology, Karlsruhe, Germany, where he is currently working toward the Ph.D. degree in electrical engineering. In 2016, he was a Research Assistant with the Department of IP and Optical Networks, Nokia Bell Laboratories, Crawford Hill, NJ, USA. His research interests include the investigation of novel optical communication system architectures and digital signal processing algorithms. He was the recipient of the Grand Prize in the annual Corning Outstanding Student Paper Competition at the Optical Fiber Communications Conference 2018.

Juned N. Kemal received the Ph.D. (Dr.-Ing.) degree in electrical engineering from the Karlsruhe Institute of Technology, Karlsruhe, Germany, in 2020, with a research focus on optical frequency combs and ultra-broadband optical interconnects. He is currently an Application and Process Development Engineer with Vanguard Automation, Karlsruhe, Germany.

Pablo Marin-Palomo received the B.S. degree in physics from the Universitat Autònoma de Barcelona, Barcelona, Spain, in 2012, and the master's degree in optics and photonics and the Ph.D. (Dr.-Ing.) degree in 2021 from the Karlsruhe Institute of Technology, Karlsruhe, Germany. He is currently a Postdoc Researcher with Brussels Photonics team, Vrije Universiteit Brussel, Brussels, Belgium, where he focuses on novel integrated light sources for THz and optical communications.

Abderrahim Ramdane received the Ph.D. degree in semiconductor physics from the University of Nottingham, Nottingham, U.K., in 1981.

He is currently with the Centre for Nanoscience and Nanotechnology, where he is working on nanostructured optical devices. In 1983, he was appointed the Head of the Solar Material Laboratory/Haut Commissariat à la Recherche, Algiers, Algeria, investigating single crystal and amorphous silicon solar cells. In 1990, he joined FRANCE TELECOM/Centre National d'Etudes des Télécommunications (CNET Bagneux) as in charge of the photonic integrated circuits on InP activity. Since 1999 he has been a Directeur de Recherche with CNRS.

Dr. Ramdane was the recipient of a two-year fellowship to investigate deep levels in III-V compounds.

Christian Koos received the Ph.D. (Dr.-Ing.) degree in electrical engineering from the University of Karlsruhe, Karlsruhe, Germany, in 2007. He is currently a Full Professor with the Karlsruhe Institute of Technology, Karlsruhe, Germany, where he is heading the Institute of Photonics and Quantum Electronics. He has co-founded several start-up companies, such as Vanguard Photonics GmbH, Vanguard Automation GmbH, SilOriX GmbH, and DeepLight SA. From 2008 to 2010, he was affiliated with the Corporate Research and Technology Department of Carl Zeiss AG in Oberkochen, Germany, where he led the technology forecast in the area of nanotechnology. He is the author of more than 140 journal papers and more than 30 patent families. His research interests include silicon photonics and hybrid integration concepts along with the associated applications in high-speed communications, optical sensing and metrology, and ultra-fast photonic-electronic signal processing. He was the recipient of several research awards and prestigious grants, such as the ERC Starting Grant in 2011 and ERC Consolidator Grant in 2017.

Wolfgang Freude (Senior Member, IEEE) received the Dipl. Ing. (M.S.E.E.) and Dr. Ing. (Ph.D.E.E.) degrees in electrical engineering from the University of Karlsruhe, Karlsruhe, Germany, in 1969 and 1975, respectively. He is currently a Professor with the Institute of Photonics and Quantum Electronics and a Distinguished Senior Fellow, Karlsruhe Institute of Technology, Karlsruhe, Germany. He has authored and coauthored more than 350 publications, coauthored a book entitled *Optical Communication*s (in German), and authored or coauthored six book chapters. His research interests include optical and wireless high-data rate transmission, high density integrated-optics with a focus on silicon photonics, photonic crystals and semiconductor optical amplifiers, and in the field of low-energy optoelectronic devices and protocols for optical access networks.

Prof. Freude is an Honorary Doctor of the Kharkov National University of Radioelectronics, Kharkov, Ukraine, and a Member of VDE/ITG and OSA. He is the General Chair of the OPTICA (formerly OSA) Advanced Photonics Congress committee Photonic Networks and Devices, and as an Editorial Board Member of the Springer Nature journal *Light: Science & Applications*.

Sebastian Randel (Senior Member, IEEE) received the Dr.-Ing. degree for his work on high-speed optical-time-division-multiplexed transmission systems from Technische Universität Berlin, Berlin, Germany, in 2005. He is currently a Full Professor with the Karlsruhe Institute of Technology, Karlsruhe, Germany, where he is co-heading the Institute of Photonics and Quantum Electronics. From 2005 to 2010, he was a Research Scientist with Siemens Corporate Technology, Munich, Germany, where he led research and standardization activities in the fields of polymer-optical-fiber communications, visible-light communications, and optical access networks. From 2010 to 2016, he was a Member of Technical Staff with Bell Laboratories, Holmdel, NJ, USA. His research focuses on the design and the implementation of power-efficient DSP algorithms for high-performance coherent optical transceivers.